ellipse like shapes. The lengths of the major and minor axis of the images could be used directly as a measure for the position of the particles in the depth direction.

2.5 Summary

The single drop impingement characteristics, the multiple drop (spray) impingement, the dynamics of the liquid surface film formed by impinging sprays and the different multicomponent planar particle velocimetry measurement techniques have been reviewed in this chapter.

First, a basis for spray impingement was made by reviewing the most important components of single drop impingement on dry and wetted surfaces, §(2.1). The key parameters that control the impingement process, the different impingement regimes and associated impingement criteria, as well as the influence of several characteristic parameters, like the drop impingement Weber number, the depth of the liquid film and the angle of impingement, were presented. Second, in §(2.2), the multiple drop impingement was presented. This section gave an overview of the experimental, numerical and theoretical studies of the interaction and impingement of two successive drops and of the spray impingement onto solid and wetted surfaces. This was followed by a survey of the aspects regarding liquid wall flows, §(2.3). Different models were reviewed of the film formed on the surface during spray impingement and an overview of the experimental studies of the wall films was given. Finally, a very broad overview of the different multicomponent planar particle velocimetry measurement techniques was presented, §(2.4). Different methods were shown for investigating the three-dimensional velocity field inside a flow by using a planar light sheet, as well as methods based on a volume illumination of the studied flow.

From this review, the conclusion can be drawn that in general the single drop and spray impingement processes can be modeled up to a certain level of accuracy. In order to raise the applicability of the existing models, the following aspects should be taken into account:

- The effect of the thin liquid surface film depth plays an important role in determining the droplet impingement outcomes. The influence of the solid surface below this surface film during impingement on the cavity characteristics has yet to be determined. It would be of great use for this parameter to be included into the analytical models for single drop impingement, to gather better numerical inputs for the characteristic time and lengths scales of the impingement processes.

- For the process of spray cooling, the minimum thickness of the surface film below the cavities during drop/spray impingement is of great importance, as this factor determines in a high degree the heat exchange between the hot solid surface and the cool liquid on top. At the moment, there is very little knowledge of this minimum film thickness in the area of spray cooling. The experimental investigation of this parameter poses many difficulties and the required measurement methods are still under development, therefore a numerical and theoretical description of this parameter is needed.

- This minimum film thickness of the surface film below the cavity after drop impingement is by a great amount being influenced by the capillary waves. These waves appear at the sides of the cavity after drop impingement and travel along the outer surface of the cavity, hereby changing its shape and influencing indirectly the liquid film below. No knowledge up to this point is known of any studies focussing in particular on these capillary waves.

- The inclusion of the surface tension and gravity in the modelling of the liquid film dynamics and cavity evolution is desirable, especially in the cases where the spreading dynamics are dominating.

- Sprays, impinging on a solid surface, generate on it a wavy liquid surface film. The modelling of the outcome of spray impingements and the dynamics of the surface film are mostly based on the superposition of single drop impingement results, where the drops have impinged on a steady liquid film. In this way, for the existing spray impingement models, the unsteady behaviour of the surface film is not taken into account. The exclusion of this important parameter results in models that do not rely on the physics associated with spray impingement, leading to an inaccurate representation of spray impingement modelling.

- In the existing spray impingement models, a certain planar film velocity is assumed. However, no knowledge is known about the magnitude of the film velocities and their fluctuations. In order to investigate these velocities accurately at different depths inside the surface film, a new measurement method needs to be developed.

All of these items will be covered in the following chapters of this thesis work by use of experimental, numerical and theoretical analyses.

Part I: Single drop impingement onto steady and wavy liquid films of finite thickness

Chapter 3

Experimental setup and measurement techniques

This chapter describes the different experimental arrangements designed to investigate the single drop impingement process onto steady and wavy liquid surface films. In order to receive the required data associated with these processes, the Shadowgraph technique has been used.

To visualise clearly the outcomes of the single drop impingement, two different experimental arrangements have been built, hence for the impingements on steady §(3.1.1) and on wavy surface films §(3.1.2)). In the case of single drop impingements on a wavy surface film, a device had to be designed to generate a wavy surface film of which the amplitude and frequency could be varied. This was required to investigate the influence of these two parameters on the impingement outcome.

The easiest way to visualise the different impingement processes, like the cavity evolution in time, is by using the Shadowgraph technique, which uses a high-speed camera in combination with a continuous or pulsed light source. The working principle, together with the adaptation to the measurement setup will be described in detail in §(3.2) for this technique.

3.1 Drop impingement layout

Theoretical and numerical spray impingement research is mostly based on models, derived from the results of single drop impingements, by making use of the superposition approach, as has been described in detail in Chapter 2. However, relying on several studies, it is clearly shown that single drop impingement data cannot be used for describing the spray impingement statistically. Sprays are a collection of a large number of drops, where the outcome of each individual drop impingement onto a liquid film is influenced by the unsteady wall film flow, as well as by the interactions with other impinging drops, both in the spray and during the interaction with the wall film, having a significant effect on the impingement process. In order to investigate the influence of the unsteady, wavy surface film on single drop impingement, by comparing the results to the case of impingement onto a steady film, two measurement arrangements are designed and built, which will be discussed below.

3.1.1 Drop impingement setup with a steady, non-moving surface film

The experimental arrangement described below is used for the investigation of the cavity appearing inside the steady liquid surface film during impingement of a single drop onto this

surface film. A schematic of the experimental setup is shown in Figure 3.1. Drops are generated using a medical push-pull syringe pump, type KDS-120 (KD Scientific Inc.), with a variable flow rate in the range of 27.8 pL/s to 0.14 mL/s. Depending on the investigated fluid, this syringe pump is programmed to dispense the liquid at a constant flow rate of about 0.40 $\mu L/s$ - 1.81 $\mu L/s$, which results in a drop frequency of about $4.54{\cdot}10^{-2}$ - $3.45 \cdot 10^{-1}$ Hz. The drop is formed and grows at the tip of the needle (Terumo Neolus, Type 20G, 0.90 × 40 mm) until its weight exceeds the net upward surface tension force of the drop and the drop detaches off the needle. To vary the drop diameter, this needle can be changed; for the single drop impingement measurements, however, the needle is kept unchanged. The rate at which the drops grow and detach can be changed by adjusting the step motor of the syringe pump. The falling drops, of which the parameters are given in §3.1.3, are enclosed in a vertical Plexiglass tube of 32 mm in diameter to protect them from air flow disturbances. To study the influence of the drop impingement velocity on the cavity evolution, the syringe pump can be changed in height with respect to the liquid surface film.

The drops pass a light barrier before impinging onto the liquid surface film, which is held by a Plexiglass cylinder of 90 mm in diameter. The impingement event is completed in a small fraction of time ($\sim O(ms)$), which is significantly smaller than the time required for the surface waves to propagate to the outer edge of the cylinder and be reflected back into the center, as its diameter is about 31 to 42 times larger than the drop diameter. In this way, the cylinder is large enough, so that wave reflections from the side of the cylinder do not interfere with the investigated impingement processes. An adequate time (2.9 - 22 s, depending on the liquid and impinging height of the impinging drops) is allowed to elapse between subsequent impingements, to assure that the surface of the target film is still before the next drop hits the surface film. The fluid of the impinging drops and that of the target surface film are the same for all the experiments. The light barrier activates an electronic delay circuit, that triggers the imaging system, consisting of two cameras, a light source and a PIV Nd:YAG laser. The details of this imaging system will be discussed in §(3.2).

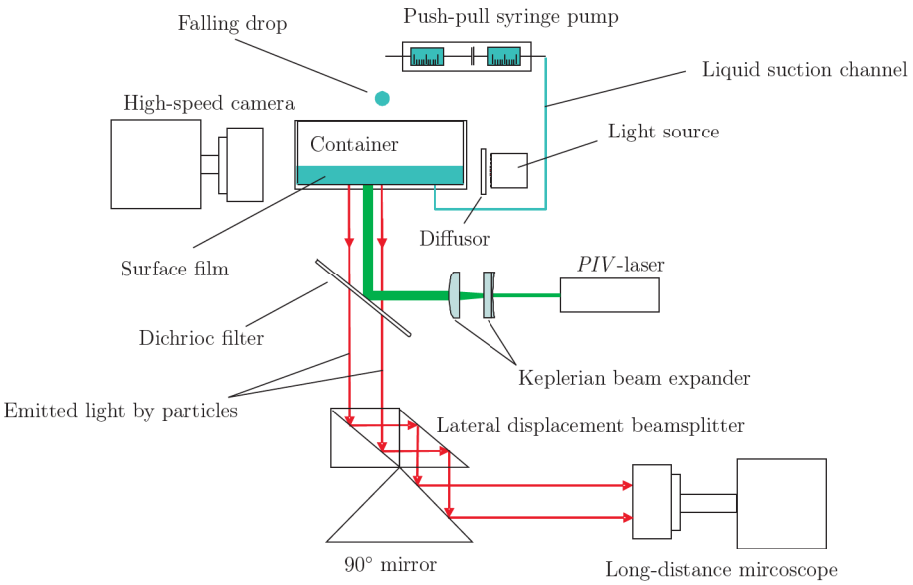

Figure 3.1: Experimental arrangement for drop impingement on a steady, non-moving surface film

3.1.2 Experimental arrangement for single drop impingement onto an unsteady, wavy surface film

The experimental arrangement described below is used for the investigation of the cavity appearing after drop impingement onto an unsteady and wavy film of finite thickness. A schematic of the experimental setup is shown in Figure 3.2.

The principle of the generation of the impinging drops is the same as has been described above for the single drop impingement onto a steady surface film. After the drops have detached off the needle of the syringe, they pass a light barrier before impinging onto the liquid surface film, which is held by a Plexiglass cube with a surface area of 100 × 100 mm.

In order to investigate the influence of the waviness of the surface film on the impingement and subsequent cavity expansion, contraction and retraction process, a plexiglass plate is positioned vertically inside the cube and connected to a vibration exciter Type 4809 (Brüel & Kjær). This vibration exciter allows a peak to peak vibration amplitude between 0 and 8 mm at a frequency range of 10 Hz to 20 kHz. The exciter is controlled by a power amplifier, Type 2718 (Brüel & Kjær), as well as by a digital delay/pulse generator, Type PDG-2510 (Directed Energy Inc.). With the amplifier the correct amplitude of the horizontally moving plate can be set, whereas the delay generator gives a time delay to the signal coming from the photodiode and used to initiate the movement of the plate. In this way, the amplitude of the wave and the phase of the wave at which the drop impinges can be set precisely, to assure a clear repeatability of the impingement process. In order to generate surface waves with different amplitudes, a lever arm is applied. The lengths of the two arms of the lever can be changed independently, due to which different maximum amplitudes of the horizontally moving plate can be achieved, resulting in surface waves with different maximum amplitudes. A large time (20 s, depending on the liquid and fall height of the impinging drops) is allowed to elapse between subsequent impingements, to assure a quiet and steady surface film before the next wave is generated. The fluid of the impinging drops and that of the target surface film are the same for all the experiments. The light barrier activates a second electronic delay circuit, that triggers the imaging system, consisting of a light source and a high-speed digital camera. The details of this imaging system will be discussed in §(3.2).

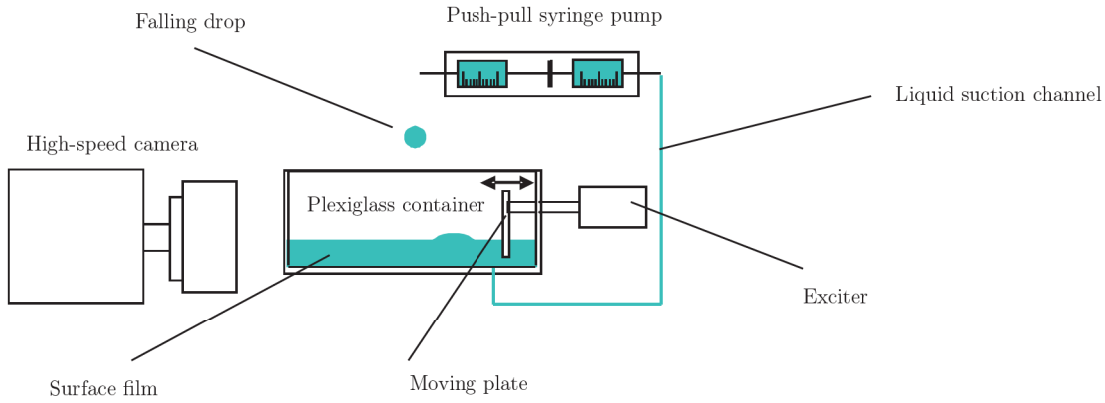

Figure 3.2: Experimental arrangement for drop impingement on a wavy surface film

3.1.3 Operating settings of single drop impingement studies

For the measurements of single drop impingements onto a steady, non-moving, as well as on an unsteady, wavy liquid surface film the same kind of parameter studies have been conducted in order to investigate the influence of different crucial parameters on the outcomes of the impingement processes. These parameters and their influences have been described in §(2.1) of chapter 2, and can be captured in several non-dimensional numbers, like the Weber number, Ohnesorge number and Reynolds number.

For the single drop impingement onto steady liquid films three liquids are used in the experiments to investigate the influence of the liquid properties on the cavity evolution in time: distilled water, isopropanol and a glycerine/water mixture consisting of 30% glycerine and 70% water. The initial diameters of the impinging drops are fixed at 2.95 ± 0.03 mm for distilled water, 2.17 ± 0.01 mm for isopropanol and 2.65 ± 0.02 mm for the glycerine/water mixture. For all the experimental investigations the same syringe needle is used to produce the drops. The difference in drop diameter between the three liquids is explained by the difference in surface tension between these fluids. As the surface tension of isopropanol is about three times smaller than of the two other liquids, the weight of the isopropanol drops exceeds faster the net upward surface tension force and the drops detach off the needle sooner.

The drop impingement velocity (i.e. the terminal velocity just before the impinging drop reaches the film surface) is calculated from a distance measurement and a preset time delay between subsequent exposures. By changing the height of the syringe pump, the impingement velocities can be varied. For distilled water this calculated impingement velocity varies from 1.68 ± 0.01 m/s and 2.88 ± 0.02 m/s, for isopropanol from 1.65 ± 0.01 m/s to 2.74 ± 0.02 m/s and for the glycerine/water mixture from 1.82 ± 0.01 m/s to 3.06 ± 0.01 m/s. For all the conducted measurements the velocity of the impinging drop is terminal. The liquid target film thickness is varied for all liquids and Weber numbers, yielding the non-dimensional film thickness of $h^* = 0.5$ to $h^* = 2$. The film thickness is held constant by means of a push-pull syringe pump, which sucks the same amount of liquid from the film as is added by the impinging drops, with an error in thickness of 3% to 7% for distilled water, 2% to 10% for isopropanol and 1% to 5% for the glycerine/water mixture. The physical properties of liquids and ranges of the non-dimensional numbers for the drop impingement studies onto steady liquid films are given in Table 3.1.

Table 3.1: Physical properties of the liquids used (at $20°C$) and the ranges of non-dimensional numbers for the single drop impingement studies onto steady liquid films

	Distilled water	**Isopropanol**	**Glycerine/water**
Density ρ $[kg/m^3]$	999	805	1,179
Viscosity μ $[kg/(m \cdot s)]$	$9.9 \cdot 10^{-2}$	$2.3 \cdot 10^{-3}$	$1.9 \cdot 10^{-2}$
Surface tension σ $[kg/s^2]$	$7.27 \cdot 10^{-2}$	$2.36 \cdot 10^{-2}$	$6.68 \cdot 10^{-2}$
Ohnesorge number Oh [-]	0.0021	0.0115	0.0406
Weber number We [-]	105 - 350	189 - 575	151 - 504
Reynolds number Re [-]	4,700 - 9,000	1,200 - 2,200	300 - 600
Froude number Fr [-]	90 - 300	120 - 380	120 - 580
Film thickness h^* [-]	0.5 - 2.0	0.5 - 2.0	0.5 - 2.0

For the experimental studies on single drop impingement onto solitary liquid waves, two liquids are used to visualise the influence of the liquid properties on the cavity evolution in time: distilled water and a glycerine/water mixture consisting of 30% glycerine and 70% water. In comparison to the impingement studies on steady liquid films, isopropanol is not used, since this fluid reacts with the glue used for the setup, due to which the setup would need to repaired after each measurement. This would lead to a modified setup for each experiment, resulting in different outcomes of the impingement processes, hence, no repeatability of the measurements would have been possible.

The initial diameters of the impinging drops are fixed at 2.90 ± 0.14 mm for distilled water and 2.57 ± 0.05 mm for the glycerine/water mixture. As mentioned already above, for all the experimental investigations the same syringe needle is used to produce the drops. For distilled water the calculated terminal impingement velocity varies from 2.66 ± 0.10 m/s and 3.12 ± 0.14 m/s and for the glycerine/water mixture from 2.50 ± 0.29 m/s to 2.99 ± 0.19 m/s. The liquid target film thickness is kept constant for all liquids and Weber numbers, yielding the non-dimensional film thicknesses of $h^* = 5.8$ and $h^* = 6.4$ with an error in the film thicknesses of less than 1% for distilled water and glycerine/water respectively.

Two kinds of waves with different amplitudes and velocities are generated in order to investigate the behaviour of the cavity on the relative wave velocity and amplitude. The wave velocities lie in between 0.311 m/s ± 0.003 and 0.392 m/s ± 0.009 for distilled water and in between 0.197 m/s ± 0.005 and 0.322 m/s ± 0.014 for the glycerine/water mixture. This results in absolute impingement velocities of the drops varying from 2.68 ± 0.10 m/s and 3.14 ± 0.14 m/s and from 2.51 ± 0.29 m/s to 3.01 ± 0.19 m/s for, respectively, distilled water and the glycerine/water mixture. The amplitudes of the waves vary for distilled water in the range from 2.26 mm ± 0.01 to 5.63 mm ± 0.02 and from 1.77 mm ± 0.01 to 5.49 mm ± 0.01 for the glycerine/water mixture, leading to the absolute fluctuating non-dimensional film thicknesses of $3.9 \leq h^*_{abs} \leq 7.7$ for distilled water and of $4.3 \leq h^*_{abs} \leq 8.5$ for glycerine/water. Since the drops always impinge on the upper part of the solitary wave, meaning the absolute film thicknesses lie above $h^*_{abs} = 4.0$, the drops always impinge on a deep pool, due to which no interaction with the bottom of the liquid film is to be expected.

To obtain measurements of the evolutions of the cavities after impingements onto different phases of the solitary waves a variable time delay between the moment at which the impinging drop passes the photodiode and the generation of the solitary wave can be set. In this way the point of impingement can be spread over the whole length of the wave. For these measurement campaigns the delay times are chosen in such a way that the impingement points are spread over the first half of the wavelength of the solitary wave, hence $0° \leq \varphi \leq 180°$. These delay times are a function of the Weber number of the impinging drop and on the liquid properties and therefore have to be defined in advance. The shortest delay time corresponds to the impingement of the drop onto the backside of the wave, hence, the receding part of the solitary wave, whereas the largest delay time sets the impingement point at the start of the rising side of the wave. The physical properties of liquids and ranges of the non-dimensional numbers and wave properties are given in Table 3.2.

3.2 Principle, data processing and adaptations of the shadowgraphy technique

Table 3.3 gives an overview of the applied measurement technique and the goals (i.e. obtained parameters) of this technique used to investigate the single drop impingement processes. The

Table 3.2: Physical properties of the liquids used (at $30°C$), the ranges of non-dimensional numbers and wave properties for the single drop impingement studies onto solitary waves

	Distilled water	**Glycerine/water**
Density ρ $[kg/m^3]$	996	1,069
Viscosity μ $[kg/(m \cdot s)]$	$7.98 \cdot 10^{-4}$	$1.86 \cdot 10^{-3}$
Surface tension σ $[kg/s^2]$	$7.12 \cdot 10^{-2}$	$6.68 \cdot 10^{-2}$
Ohnesorge number Oh [-]	0.0018	0.0019
Weber number We [-]	235 - 521	134 - 413
Reynolds number Re [-]	8,300 - 13,300	7,200 - 11,000
Froude number Fr [-]	210 - 410	160 - 450
Undisturbed film thickness h^* [-]	5.8	6.4
Wave velocity U_w $[m/s]$	0.311 - 0.392	0.197 - 0.322
Wave amplitude A_w $[m]$	$2.26 \cdot 10^{-3}$ - $5.63 \cdot 10^{-3}$	$1.77 \cdot 10^{-3}$ - $5.49 \cdot 10^{-3}$
Wave phase[1] φ [°]	20 - 179	12 - 166
Absolute drop velocity[1] $U_{d,abs}$ $[m/s]$	2.68 - 3.14	2.51 - 3.01
Absolute film thickness $h^*_{abs}[-]$	3.9 - 7.7	4.3 - 8.5

[1] at impingement

shadowgraphy technique is a standard measurement technique, described very well in literature. In the detailed survey given below, only a short overview of the working principle of this technique will therefore be given, as well as the adaptation of the technique to the aims of the study of the impingement processes and the analysis of the recorded data.

Table 3.3: Overview of the applied measurement technique

Technique	**Goal**	**Comments**
Shadowgraphy	Qualitative visualisation of impingement processes and of spray cones	Qualitative, time-resolved, integrated along line-of-sight

3.2.1 Working principle

Shadowgraphy, or backlight-technique, is a relatively simple, but at the same time powerful tool to perform qualitatively high investigations of the impingement processes and spray processes and is therefore often applied. Here, the visualisation technique is chosen for its simplicity and due to the fact that no tracer particles in the liquids are needed. The physical principles used for these investigations are the scattering of light by the drops in the sprays, as well as the refraction of the incident light due to the density gradients between the liquid and the gas phase. The signals, that are recorded by the camera, are integrated over the distance between the light source and the camera. Therefore, the three-dimensional effects cannot be resolved, unless multiple cameras are used simultaneously.

3.2.2 Adaptation to the measurement requirements

For the investigation of the impingement process for single drop impingements onto steady and onto wavy surfaces, two different shadowgraphy arrangements are used. The main goals of the shadowgraphy technique for these investigations are to capture the diameter and impingement velocity of the falling drops, combined with the temporal and spatial evolution of the cavity appearing below the surface of the liquid target film after impingement; hence to visualise the growing and receding process of the cavity.

The employed configuration for the single drop impingement investigation on a steady, non-moving film is given in Figure 3.1. A LED-stroboscope from StroboLED is used to illuminate the impingement process. A flash duration of 10 μs is set, as the flashes must be as short as possible to freeze the impingement process at different instants in time, but long enough to generate enough light for the recordings. To assure a uniform diffused illumination, a diffusor glass plate with a uniform gray intensity is set inbetween the stroboscope and the Plexiglass container. A high-speed CMOS HCC-1000 camera from Vosskühler GmbH with 1024 $\times$ 1024 pixels, fitted with an extended 50 mm focal length Cosmicar Television Lens for a good balance between the required spatial resolution and the necessary field of view, is used as detector. An exposure time of 2.2 ms is set, but due to the flash duration of only 10 μs the recordings are not integrated over time.

Quasi-simultaneously a second shadowgraphy system is applied. This method detects the reflection gradients caused by the impinging drop interacting with the target film, as well as by the surface capillary waves traveling radially outwards away from the point of impingement. In order to obtain good qualitative measurements, it requires the light source, the object to be observed and the detector to be on a straight line. A New Wave Solo PIV III double-pulsed Nd:YAG laser (λ = 532 nm, 30 mJ/pulse) is used for the illumination. The laser pulses are expanded in diameter using a Keplerian beam expander up to a diameter of 11 mm, reflected by a dichroic filter placed under 45° and directed upwards, where they pass the investigated flow orthogonally. The laser light, reflected by the surface film, passes the dichroic filter and is recorded by a PCO Sensicam 12-bit CCD camera with 1280 $\times$ 1024 pixels. This camera is equipped with a long distance microscope (Nikon Nikkor 105 mm focal length lens together with a 160 mm extension tube). The exposure of the camera is set to 5 μs to assure sharp recordings, whereas the time between the two recordings is 1 μs. Both methods lead to images with a high spatial resolution of 18.9 $\mu m/pix$ (field of view (FOV) of 19.4 $\times$ 19.4 mm) and 5.6 $\mu m/pix$ (FOV 7.2 $\times$ 5.7 mm) for, respectively, the CMOS camera and the Sensicam camera.

As soon as the falling drop passes the light barrier, a signal is transmitted to an electronic digital delay generator, where the time delay is set between the input signal and the outgoing one. The delayed signal is then passed to the frame grabber of the PIV system from Dantec Dynamics, as well as to the CMOS camera. In this way, the PIV laser, the Sensicam, the CMOS camera and the LED stroboscope are all triggered at the same time instant. The recording process is as follows: the CMOS high-speed camera takes typically 100 images of a single impingement process with a time delay of 2.16 ms (i.e. at a recording frequency of 462 Hz) between individual exposures. With the use of an extra internal time delay, the Sensicam takes two images at an exact pre-determined time during the impingement process, resulting in an image at the last time instant before impingement and one at the first time instant after impingement. In this way, a verification of the exact moment at which the drop impinges onto the target film is given. Each recording is then repeated five times, after which the delay generator is changed 54 times in steps of 40 μs to cover the whole time span of the impingement process.

For the study of the cavity appearing after impingement on an unsteady, wavy film, the optical configuration is shown in Figure 3.2. Here, as well as for the detailed investigation of the capillary waves moving along the outer surface of the cavity for impingement on a steady, non-moving film, the shadowgraphy technique is used as well. However, in comparison to the arrangement described above, an Arrilux 400 light source, equipped with a 400 W metal halide lamp from Arnold & Richter Cine Technik, together with the Fastcam SA1.1 high-speed camera from Photron is used. The light source generates continuous light and is equipped with either a spot filter (10° light cone angle) or a narrow-flood filter (10° - 20° light cone angle). The Fastcam has a resolution of 1024 × 1024 pixels, but depending on the recording frequency to capture all the details of the impingement processes, this resolution can be set lower. For these investigations this camera is equipped with an extended 85 mm focal length Nikon Nikkor lens together with a 71.5 mm extension tube, working as a long distance microscope. This leads to a spatial resolution of the images of 23.2 $\mu m/pix$ (field of view (FOV) of 23.8 × 23.8 mm).

The triggering of the Fastcam follows over an electrical signal, transmitted as soon as the falling drop passes the light barrier. The camera records the studied impingement process with a frequency of 5,400 Hz, resulting in an image every 185 μs, together with an exposure time of 1 μs. Every recording sequence is repeated five times, in order to verify the repeatability of the measurements and to assure a low scattering of the data afterwards.

For the spray impingement measurements, which will be described in Chapter 6, the spray has first to be characterised, to get a detailed overview of its characteristics before impingement. The shadowgraphy technique is an excellent tool to receive qualitative images of the spray cone and the change of this cone for different liquid volume flows, with and without air as a carrier gas. The employed configuration is shown in Figure 3.3.

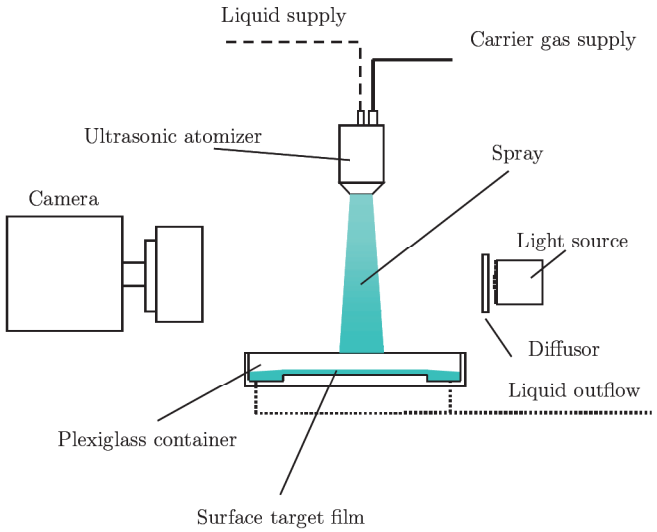

Figure 3.3: Sketch of the shadowgraphy technique setup for the visualisation of the spray cone

The Arrilux 400 light source from Arnold & Richter Cine Technik, equipped with a 400 W metal halide lamp and with either a spot filter (10° light cone angle) or a narrow-flood filter (10° - 20° light cone angle) is used for illumination. The light, reflected and refracted by the drops of the spray, is recorded by a PCO Sensicam 12-bit CCD camera with 1280 × 1024 pixels. This camera is equipped with a Nikon Nikkor 85 mm focal length lens. The exposure of the camera

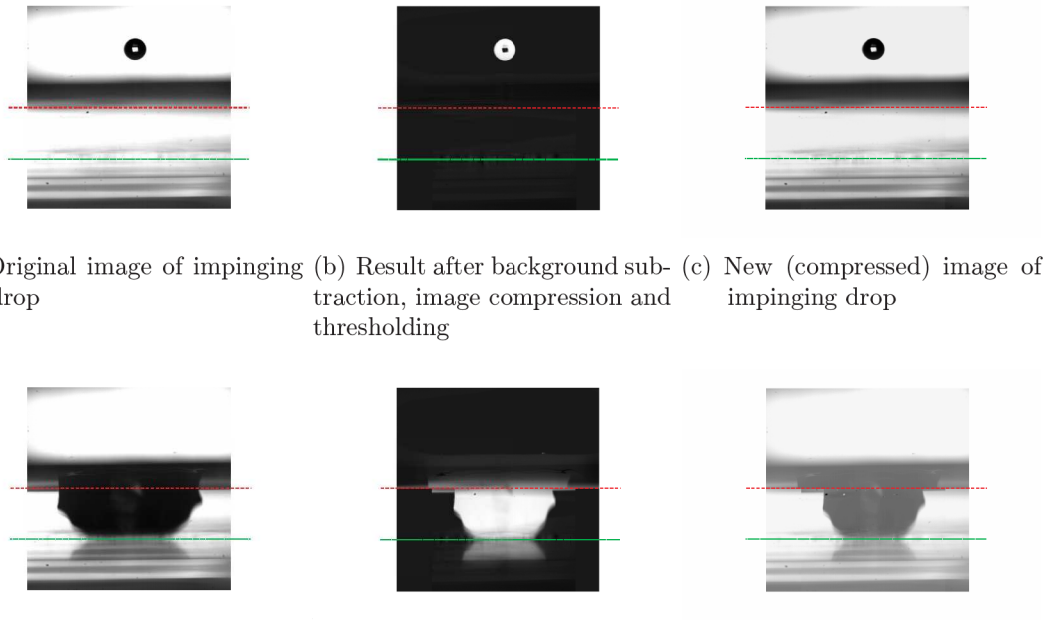

(a) Original image of impinging drop

(b) Result after background subtraction, image compression and thresholding

(c) New (compressed) image of impinging drop

(d) Original image of cavity

(e) Result after background subtraction, image compression and thresholding

(f) New (compressed) image of cavity

Figure 3.4: Compensation of image magnification differences above and below the surface of the target film for the shadowgraph images (▪ ▪ : surface of target film; ▬ : bottom of the film)

is again set to 5 μs to assure sharp recordings. This results in images with a spatial resolution of 150 $\mu m/pix$ (field of view of 192 $\times$ 154 mm) for the US10 atomizer and 152 $\mu m/pix$ (field of view of 195 $\times$ 156 mm) for the US20 nozzle.

3.2.3 Image processing of shadowgraph recordings

An automatic image processing tool based on Matlab is used to extract information about the properties of the impinging drop (diameter, velocity, eccentricity) and the cavity appearing below the film surface after impingement (shape and size), as well as the shape of the spray cone. After background subtraction, a threshold is laid over the images to obtain binary images and to extract out of these images only the desired information. The threshold value is determined by analysing the gray intensity distributions of all images per recording. A mean grey intensity distribution over all the images is calculated, of which an histogram is made. The peak of this histogram, hence the grey scale intensity with the most entries, is set as the background intensity. Either this value of the grey scale intensity is taken directly as the threshold value, or, if necessary, a fraction of the difference between the maximum grey scale and the background intensity is added to increase the threshold with a few percent. As the background above and below the liquid surface is very good to perfectly homogeneous, this threshold can be set well.

For the drop impingement images onto a steady liquid film an extra subroutine is written, as the drops impinge on a surface film, that is held inside a circular Plexiglass container. Due to the different indices of refraction of the air and the liquid of the target film, in combination with a curved surface of the Plexiglass container, the part of the image below the liquid surface is

being magnified on the recordings in comparison to the part above the liquid surface. Therefore the magnification factor above and below the film surface are not the same. To compensate for this difference in magnification, as well as for the possible misalignment of the camera with the central axis of the Plexiglass container - leading to a horizontally shifted cavity with respect to the impinging drop -, each binary image is split up into three parts: the part above the liquid surface, the part below the liquid surface, left from the vertical center axis of the cavity, and the part below the liquid surface, right from the vertical center axis of the cavity. The segment of the image above the liquid surface is untouched, whereas the two parts below the surface are first shifted horizontally to assure that the center line of the cavity is aligned with the center line of the impinging drop, after which both parts are "compressed" in such a way, that the magnification factor below the film surface corresponds to that above the film (Figure 3.4(b) and 3.4(e)). To obtain the original images, the background is added again to the "compressed" images (3.4(c) and 3.4(f)). By comparing the size of the cavity between Figure 3.4(d) and Figure 3.4(f), the compression of the cavity can be seen clearly.

3.3 Summary

In this chapter the different experimental arrangements designed to investigate the single drop impingement processes have been presented. In order to visualise clearly the impingement outcomes, two different experimental arrangements have been designed: the first one to investigate the impingement onto a steady film §(3.1.1), the second one to study the influence of the unsteady, wavy surface film on single drop impingement §(3.1.2).

The shadowgraph measurement technique (§(3.2)) has been described to account for the acquisition of several measurement parameters, like the time evolution of the cavity after drop impingement and the corona appearing above the liquid film. Of this measurement technique the working principle has been explained, followed by the adaptation of the technique to the experimental arrangements in order to acquire the desired measurement data. The associated data analysis and post-processing have been presented as well.

Together with the previous chapter, a detailed overview of the physics of the parameters influencing single drop impingement processes as well as the acquisition methods for these parameters have been presented. The acquired data of the different impingement studies and the analytical models to predict the outcomes of the impingement processes are subject of the next chapters.

Chapter 4

Single drop impingement onto a liquid film of finite thickness

The previous chapters were intended to give a detailed overview of the single drop impingement characteristics, the multiple drop and spray impingement outcomes, as well as of the dynamics of the liquid surface film formed by impinging sprays, by means of experiments, numerical simulations and analytical calculations. A basis for spray impingement was made by reviewing the most important components of single drop impingement on dry and wetted surfaces. The key parameters that control the impingement process, the different impingement regimes and associated impingement criteria, as well as the influence of several characteristic parameters, like the drop impingement Weber, Reynolds and Froude numbers, the depth of the liquid film and the angle of impingement, were presented.

It was shown that, relying on several studies, single drop impingement data cannot be used for describing the spray impingement process statistically. Sprays are a collection of a large number of drops, where the outcome of each individual drop impingement onto a liquid film is influenced by the unsteady wall film flow, as well as by the interactions with other impinging drops, both in the spray and during the interaction with the wall film, all of them having a significant effect on the spray impingement process. In order to investigate the influence of the unsteady, wavy surface film on the outcome of the single drop impingement process, by comparing the results with the case of single drop impingement onto a steady film, two measurement arrangements were built (§(3.1)). To visualise clearly the outcomes of the single drop impingement processes on steady and wavy liquid surfaces, the high-speed shadowgraphy technique was applied, explained in detail in §(3.2).

In this chapter the results of the single drop impingement processes onto steady liquid films of finite thickness will be presented. For the impingement results onto steady liquid films, first of all a comparison of the observations of the impingement process for different parameters will be shown. These parameters are the initial liquid film height h^*, made non-dimensional by the impinging drop diameter D_d, the terminal velocity of the drop before impingement U_d, captured in the Weber number We, and the properties of the liquids used, hence the surface tension and viscosity. The influence of the liquid properties are commonly expressed by two non-dimensional numbers, the Weber number and the Reynolds number, for respectively the influence of the surface tension and the viscosity. These parameters have been changed during the measurement campaigns to investigate their influence on the outcomes of the impingement process. This parametric study is done in order to evaluate the influences of these different key impingement parameters on the cavity behaviour in time. Several observations on the velocity

with which the cavity penetrates into the liquid film, the shape of the cavity in time, the times of receding and retraction of the cavity, the capillary waves and on the central jet are made.

In the next paragraphs the impingement process, in particular the evolution of the cavity, will be analysed in more detail. The evolution of the depth of the cavity, by measuring its lowest point, will be analysed and compared for different drop impingement parameters and film thicknesses. The same analysis will be conducted on the diameter evolution of the cavity at half the film thickness, in order to investigate the maximum cavity diameter and the time at which this maximum diameter is reached. The minimum thickness of the residual liquid surface film, still present below the cavity, will be presented, which is a key parameter for understanding the heat flux for spray cooling.

The results of the experiments will be compared with the analytical models and the numerical simulations in order to evaluate these models and the numerical codes. The residual film thicknesses, present below the cavities at the moment the cavities reach their maximum depths, will be presented as well and compared with a mathematical model. The values of all of these parameters give an idea of the typical time and length scales that are important when investigating and modeling sprays, for example for spray cooling.

4.1 Single drop impingement onto steady liquid films

In this paragraph the observations of the single drop impingement onto steady liquid films of finite thickness are presented. For the parametric studies different parameters of the impinging drop and of the liquid film are changed, in order to study their influences on the cavity behaviour in time. These parameters are the initial liquid film height h^*, the Weber number, hence, the terminal velocity of the drop before impingement, and the liquid properties (viscosity and surface tension). Nine of the many impingement experiments are selected and presented hereafter. The impingement parameters of these experiments are given in Table 4.1.

Table 4.1: Parameters of the selected experiments used for discussion of the time evolution of the cavity upon impingement onto a steady liquid film

Liquid	h^*	**We**	**Fr**	**Re**
Distilled water	0.5	317	291	8,170
Distilled water	1.5	348	276	8,883
Distilled water	2.0	114	91	5,061
Distilled water	2.0	225	180	7,118
Distilled water	2.0	350	273	8,931
Distilled water	2.5	344	280	8,774
Distilled water	6.4	291	296	9,307
Isopropanol	2.0	527	366	1,982
Glycerine/Water	2.0	505	399	561

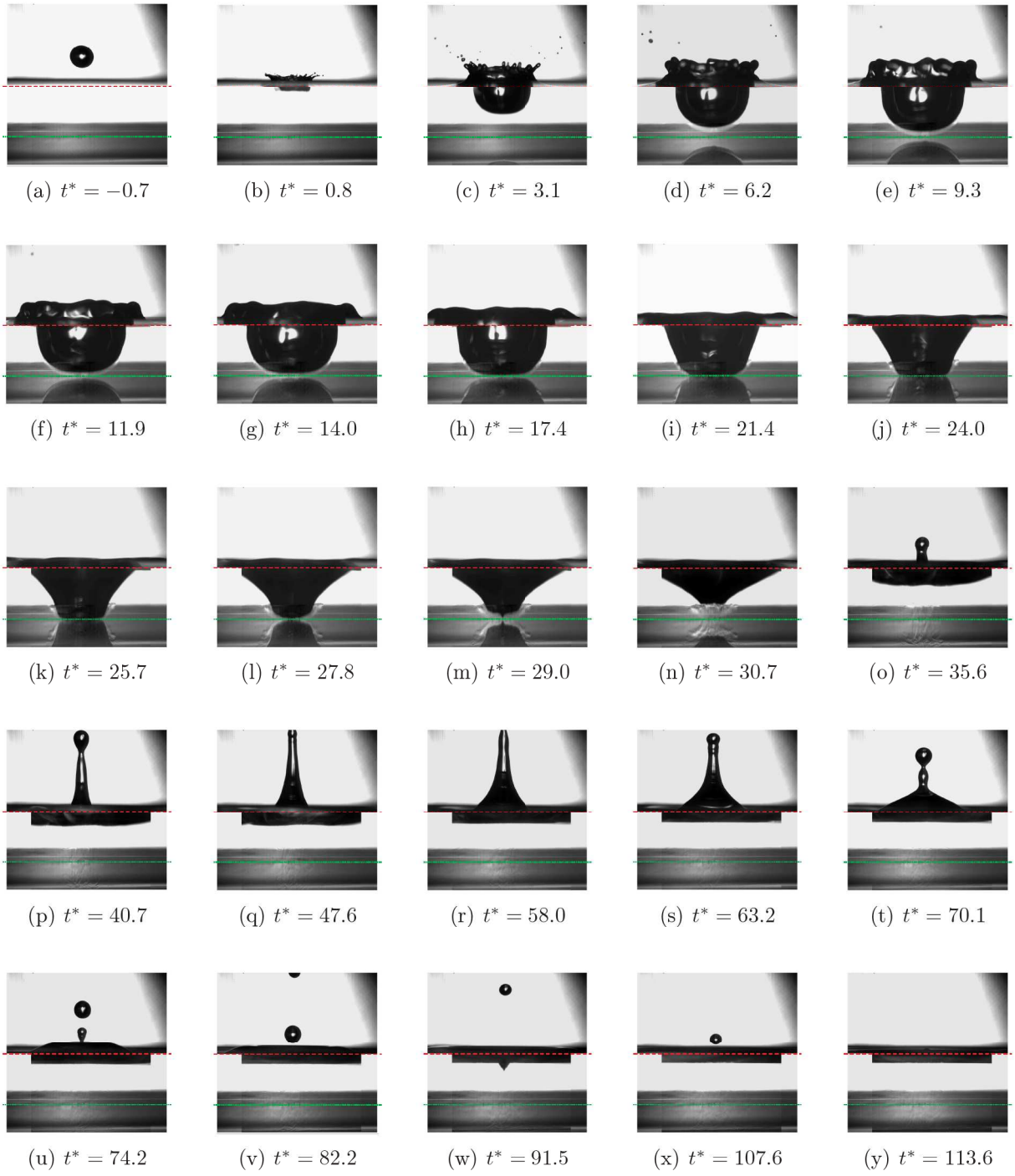

(a) $t^* = -0.7$ (b) $t^* = 0.8$ (c) $t^* = 3.1$ (d) $t^* = 6.2$ (e) $t^* = 9.3$

(f) $t^* = 11.9$ (g) $t^* = 14.0$ (h) $t^* = 17.4$ (i) $t^* = 21.4$ (j) $t^* = 24.0$

(k) $t^* = 25.7$ (l) $t^* = 27.8$ (m) $t^* = 29.0$ (n) $t^* = 30.7$ (o) $t^* = 35.6$

(p) $t^* = 40.7$ (q) $t^* = 47.6$ (r) $t^* = 58.0$ (s) $t^* = 63.2$ (t) $t^* = 70.1$

(u) $t^* = 74.2$ (v) $t^* = 82.2$ (w) $t^* = 91.5$ (x) $t^* = 107.6$ (y) $t^* = 113.6$

Figure 4.1: Single drop impingement onto a liquid layer of non-dimensional thickness $h^* = 2$. The evolution of the cavity formed by a distilled water drop ($We = 350$, $Fr = 273$, $Re = 8,931$) impingement at various non-dimensional time instants. The impingement parameters are $D_d = 3.1$ mm and $U_d = 2.9$ m/s

4.1.1 Evolution of the cavity in time

In Figure 4.1 the evolution of the cavity appearing after impingement of a distilled water drop onto a steady liquid film of distilled water of thickness $h^* = 2$, is presented at various non-dimensional times t^*. In this figure, as well as in all the figures presented hereafter, $t^* = 0$ corresponds to the time at which the impinging drop has first contact with the liquid film, whereas the red and green dashed lines are the surface of the liquid film and the bottom of liquid film respectively. With the use of this figure the mechanism of drop impingement onto a liquid layer of finite thickness can be subdivided into several phases:

i *Drop impingement onto the surface of the liquid film and its initial deformation*, Figure 4.1(a) and 4.1(b).

ii *Prompt splash*, Figure 4.1(b) and 4.1(c). In these figures it can be seen that the prompt splash mechanism leads to the almost immediate formation of very small jets and secondary droplets. Whether the prompt splash takes place and how many small jets and secondary droplets appear depends on the impinging drop Weber number and of the liquid properties, as will be discussed in a later part of in this chapter.

iii *Formation of a cavity*, Figure 4.1(c). The cavity is formed inside the liquid film by the kinetic energy of the impinging drop, pushing away the liquid of the surface film. The liquid of the impinging drop itself is spread over the inner surface of the cavity, Figure 4.2.

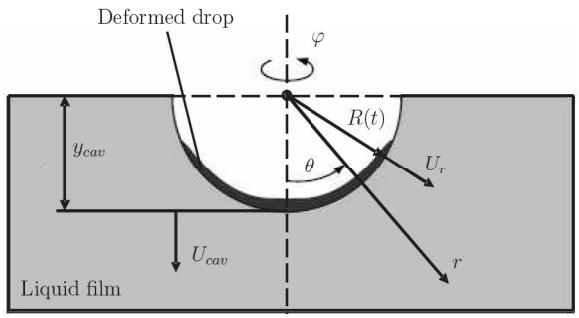

Figure 4.2: Sketch of the penetrating cavity

Due to the difference in refraction indices of the liquid and the air the cavity appears dark in the images recorded by the shadowgraphy technique. At the same time a crown-like sheet, the so-called corona, bounded by a rim, is formed above the surface of the liquid film. This corona is formed by the liquid of the surface film, being pushed upwards by the impinging drop. The rim of the corona can become unstable due to three-dimensional oscillations, resulting in the break-up of the rim into finger-like jets, Figure 4.4(a). These fingers can in turn also become unstable, leading to secondary droplets flying away.

iv *Expansion of the cavity*, Figure 4.1(d) to 4.1(f). At these time instants the cavity expands both in diameter as well as in depth, thereby converting the kinetic energy of the impinging drop into surface tension energy and dissipated energy. For impingements upon surface films of finite thickness, like is the case here, the bottom of the cavity reaches at a certain

time the bottom of the liquid film, Figure 4.1(f). From this time instant on, the cavity cannot expand further in depth, but will continue growing in diameter until the point at which all kinetic energy has been converted into surface tension energy and dissipated energy.

v *Appearance of the capillary waves*, Figure 4.1(g) and 4.1(h). These rather sharp capillary waves appear on the surface of the cavity, Morton *et al.* [100], Jong-Leng [66], Zhang and Thoroddsen [200]. They are created at the inside of the corona at the time instant at which the rim, falling back onto the liquid surface due to gravity, merges with the liquid film. Exactly at this time instant the pressure inside the rim is elevated, corresponding to the curvature of the rim and its acceleration (Beberovic *et al.* [10]). The outer corners of the capillary waves are rather sharp, indicating strong local pressure drops. The capillary waves separate high pressure regions above the waves from relatively low pressure regions below the waves. Due to these high pressure regions the shape of the cavity gets deformed when the wave passes. The pressure differences ahead of and behind the capillary waves lead to the liquid acceleration and enhance the wave propagation, due to which the capillary waves move downwards along the cavity surface, thereby accelerating when approaching to the bottom of the cavity. For liquids with low surface tensions trains of capillary waves can be observed, see for example Figure 4.4(l), where three capillary waves can be seen. The front capillary waves are usually small in amplitude, whereas the last capillary waves have an increased amplitude and wave velocity.

vi *Receding and merging of the cavity*, Figure 4.1(i) to 4.1(l). Due to the surface tension forces acting on the cavity surface, as well as the downward movement of the capillary waves, the cavity changes its shape from a hemisphere to a conical shape. The capillary waves merge at the bottom of the cavity, leading to a sharp bottom of the cavity, where high pressure differences and surface tension forces are present.

vii *Retraction of the cavity and emergence of a central jet*, Figure 4.1(m) to 4.1(r). Due to the high pressure differences and surface tension forces at the bottom of the cavity the cavity is pushed upwards, hence, retracting from the bottom of the liquid layer. As a result of the velocity with which the center of the cavity retracts, a central jet is formed. The thickness and the maximum height of the central jet, as well as the diameter and maximum height of the secondary droplets pinching-off the central jet, are a function of the impinging drop Weber number, the initial film thickness and the liquid properties, Shin and McMahon [153].

viii *Impingement of secondary droplets*, Figure 4.1(s) to 4.1(y). Due to gravity the secondary droplets, pinched-off the central jet, fall back onto the liquid surface. Depending on the impingement velocity of these secondary droplets, they can either create a second impingement process, thereby repeating the complete impingement process described above, however, with a smaller cavity as a result (Figure 4.1(w)), or, when the velocity of the impinging droplets is relatively small, they can bounce on the liquid surface and subsequently coalesce with it.

4.1.2 Influence of liquid film height on cavity shape

Consider the impingement of a very sparse spray onto a thin liquid film. Since for this spray the frequency with which the drops impinge onto the surface film is relatively low, the film is given enough time to recover to its initial stage after each impingement. This implies that each

drop of the spray "sees" an undisturbed liquid film of constant height.

Most common sprays, however, are rather dense, meaning that the impingement frequency at one certain point inside the surface film is relatively high. This means that the chance a certain drop of the spray impinges onto the cavity, formed by a former drop impingement, is also relatively high. The second drop "sees" therefore at its impingement not the undisturbed liquid film with constant thickness, but a disturbed surface film having a smaller thickness.

This process implies a thorough study of the impingement of single drops onto liquid surface films of various thicknesses, in order to investigate its influence on the cavity behaviour in time. The results of this part of the study on the outcome of the single drop impingement process are shown in the Figures 4.3 and 4.4. The impingements onto six different liquid film heights in the range of $h^* = 0.5$ to $h^* = 6.4$ are investigated. The outcomes of the single drop impingements for distilled water onto four of these liquid film heights ($h^* = 0.5$, $h^* = 1.5$, $h^* = 2.5$ and $h^* = 6.4$) are shown in these figures. The classification for the different film height regimes, given by Tropea and Marengo [170], defines that $h^* = 0.5$ and $h^* = 1.5$ are liquid films, $h^* = 2.5$ is a shallow pool and $h^* = 6.4$ a deep pool. For each of these measurements the Weber number, Froude number and Reynolds number of the impinging drops are in the same range. Figure 4.3 shows the drop impingement outcomes inbetween the non-dimensional times $t^* = -0.7$ and $t^* = 11.9$ and Figure 4.4 for the times inbetween $t^* = 17.4$ and $t^* = 40.7$.

Until $t^* = 3.1$ no clear differences between the impingement outcomes can be seen for different film heights. At $t^* = 3.1$ the formation of the cavity below the liquid surface is observed for all four film heights. Since the cavity for each of the film heights grows in depth with a constant velocity, as will be shown in the next paragraph, the cavity for the film height $h^* = 0.5$ reaches at this time instant already the bottom of the liquid film. This leads to a shape of the cavity that is elongated in the radial direction, hence, an oblate cavity. For the other film heights each cavity is close to hemispherical. After each impingement a prompt splash is observed, resulting in many very small jets and secondary droplets, and the corona is seen to be formed.

The cavities for $h^* = 2.5$ and $h^* = 6.4$ continue to increase in radial direction at the time instants $t^* = 9.3$ and $t^* = 11.9$, whereas at the first time instant the cavity for $h^* = 1.5$ reaches the bottom of the liquid film. Just as for $h^* = 0.5$ this cavity can no longer increase in depth; it only increases in the film radial direction until the point at which all kinetic energy of the impinging drop has been converted into surface tension energy and dissipated energy. During these non-dimensional times the rim for $h^* = 0.5$ becomes unstable and large finger-like jets are appearing, whereas for the other liquid films the rims remain stable.

The capillary waves appear for all four film heights at the same non-dimensional time of $t^* = 17.4$ and move downwards along the surface of the cavity, changing its shape downstream of the capillary waves, see the images at $t^* = 24.0$. At the same time the cavities recede and contract due to the surface tension forces, changing their shapes from hemispherical to conical. It is observed that the cavity for $h^* = 2.5$ reaches the bottom of the liquid film not before the capillary waves have met at the bottom of the cavity, Figure 4.4(g). This means that for this film height still a brief, but clear contact is observed between the cavity and the bottom of the liquid film, although its influence on the impingement outcome is thought to be small. For film thicknesses larger than $h^* = 2.5$ no interaction between the cavity and the bottom of the pool is observed; hence, the region of impingement onto deep pools is entered.

After the time instant at which the capillary waves have reached the bottom of the cavity, the cavity starts to retract. The time instant of the start of the cavity retraction is independent of the film depth for finite liquid films up to $h^* = 2.5$, although some small differences

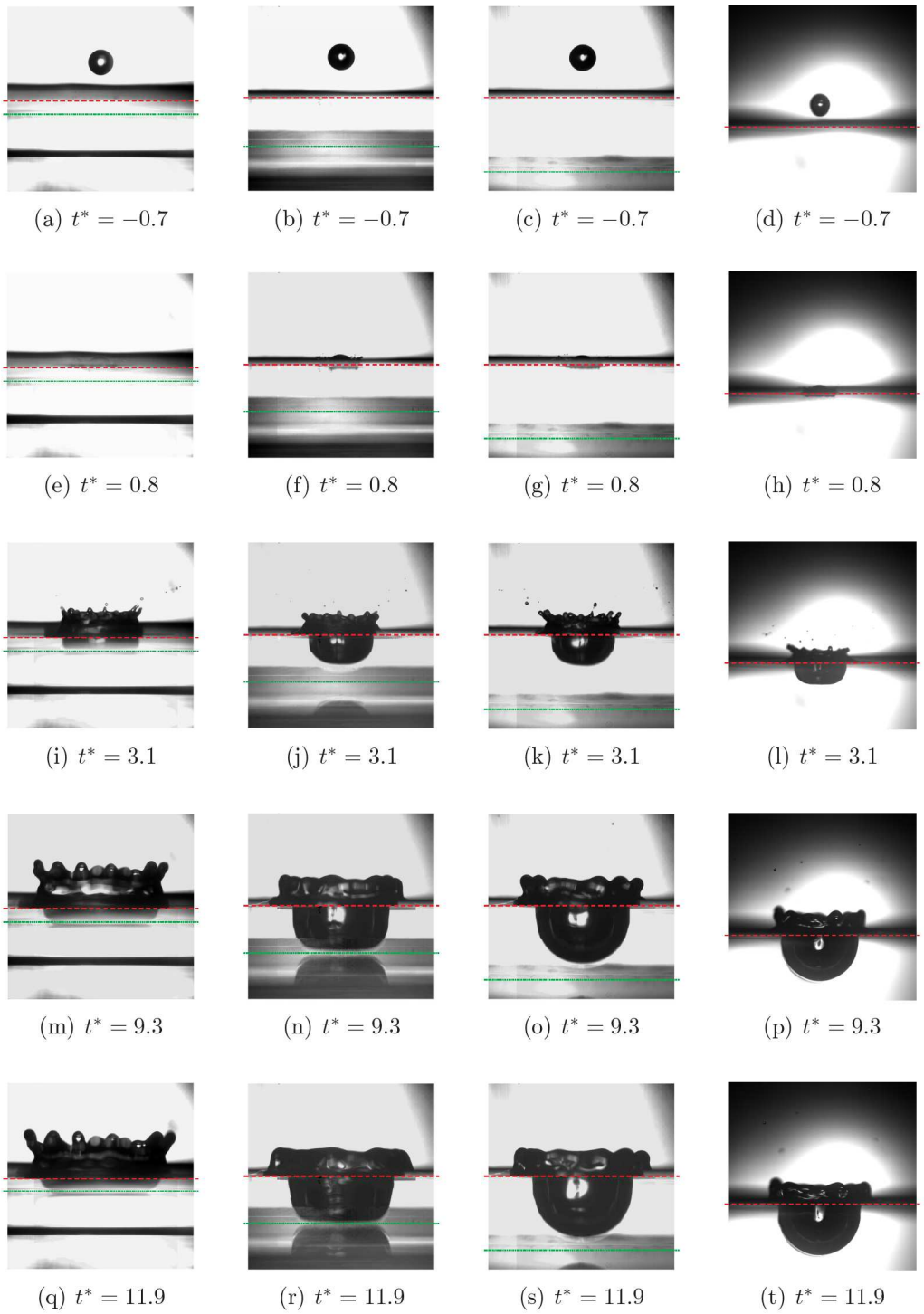

(a) $t^* = -0.7$ (b) $t^* = -0.7$ (c) $t^* = -0.7$ (d) $t^* = -0.7$

(e) $t^* = 0.8$ (f) $t^* = 0.8$ (g) $t^* = 0.8$ (h) $t^* = 0.8$

(i) $t^* = 3.1$ (j) $t^* = 3.1$ (k) $t^* = 3.1$ (l) $t^* = 3.1$

(m) $t^* = 9.3$ (n) $t^* = 9.3$ (o) $t^* = 9.3$ (p) $t^* = 9.3$

(q) $t^* = 11.9$ (r) $t^* = 11.9$ (s) $t^* = 11.9$ (t) $t^* = 11.9$

Figure 4.3: Single drop impingement onto a liquid layer of different non-dimensional thicknesses between $h^* = 0.5$ and $h^* = 6.4$. The evolution of the cavity formed by a distilled water drop impingement at non-dimensional time instants between $t^* = -0.7$ and $t^* = 11.9$. The impingement parameters are (left) $D_d = 2.9$ mm and $U_d = 2.9$ m/s ($We = 317$, $Fr = 291$, $Re = 8,170$) for $h^* = 0.5$; (middle left) $D_d = 3.1$ mm and $U_d = 2.9$ m/s ($We = 348$, $Fr = 276$, $Re = 8,883$) for $h^* = 1.5$; (middle right) $D_d = 3.0$ mm and $U_d = 2.9$ m/s ($We = 344$, $Fr = 280$, $Re = 8,774$) for $h^* = 2.5$ and (right) $D_d = 2.7$ mm and $U_d = 2.8$ m/s ($We = 291$, $Fr = 296$, $Re = 9,307$) for $h^* = 6.4$

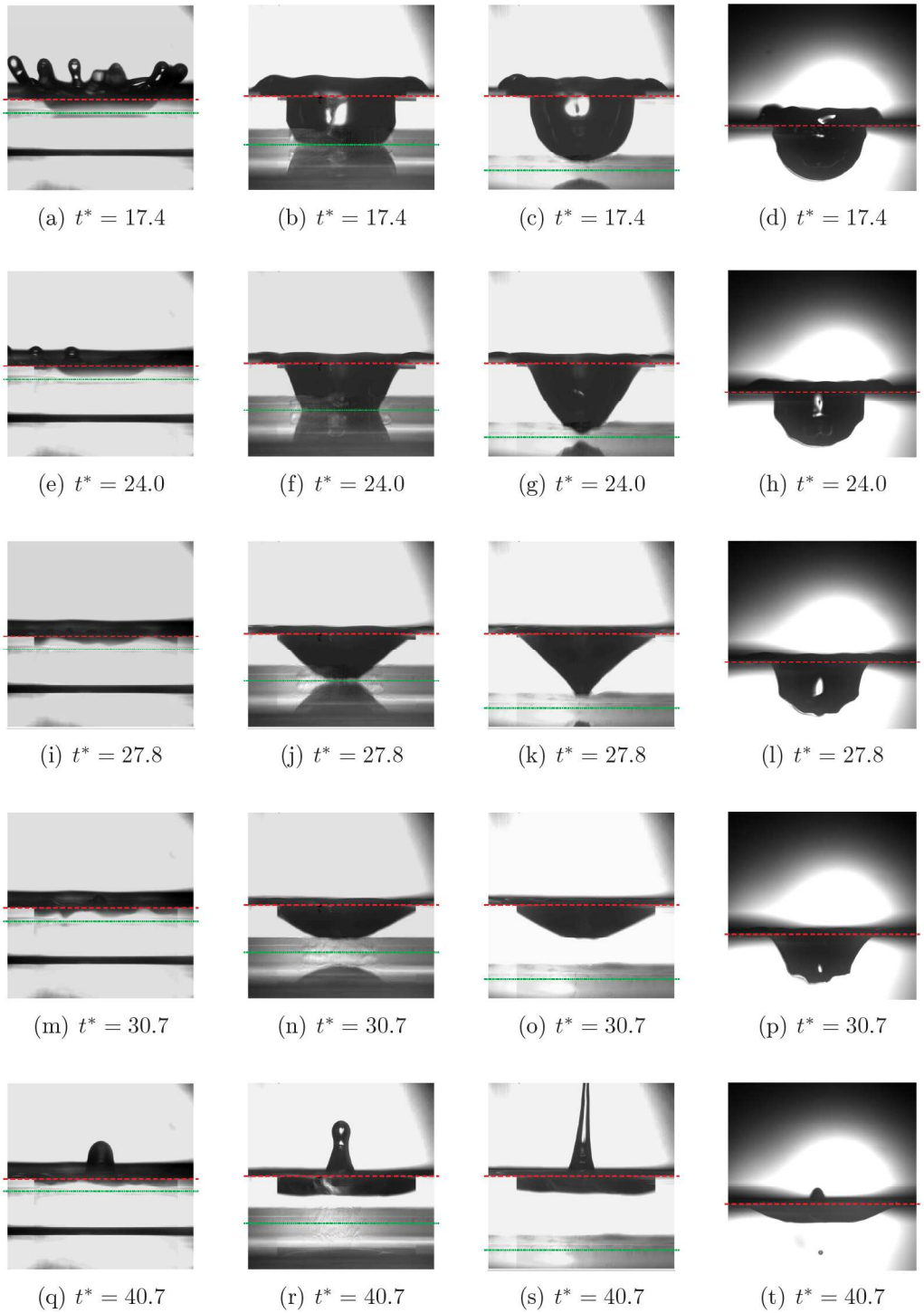

(a) $t^* = 17.4$ (b) $t^* = 17.4$ (c) $t^* = 17.4$ (d) $t^* = 17.4$

(e) $t^* = 24.0$ (f) $t^* = 24.0$ (g) $t^* = 24.0$ (h) $t^* = 24.0$

(i) $t^* = 27.8$ (j) $t^* = 27.8$ (k) $t^* = 27.8$ (l) $t^* = 27.8$

(m) $t^* = 30.7$ (n) $t^* = 30.7$ (o) $t^* = 30.7$ (p) $t^* = 30.7$

(q) $t^* = 40.7$ (r) $t^* = 40.7$ (s) $t^* = 40.7$ (t) $t^* = 40.7$

Figure 4.4: Single drop impingement onto a liquid layer of different non-dimensional thicknesses between $h^* = 0.5$ and $h^* = 6.4$. The evolution of the cavity formed by a distilled water drop impingement at non-dimensional time instants between $t^* = 17.4$ and $t^* = 40.7$. The impingement parameters are (left) $D_d = 2.9$ mm and $U_d = 2.9$ m/s ($We = 317$, $Fr = 291$, $Re = 8,170$) for $h^* = 0.5$; (middle left) $D_d = 3.1$ mm and $U_d = 2.9$ m/s ($We = 348$, $Fr = 276$, $Re = 8,883$) for $h^* = 1.5$; (middle right) $D_d = 3.0$ mm and $U_d = 2.9$ m/s ($We = 344$, $Fr = 280$, $Re = 8,774$) for $h^* = 2.5$ and (right) $D_d = 2.7$ mm and $U_d = 2.8$ m/s ($We = 291$, $Fr = 296$, $Re = 9,307$) for $h^* = 6.4$

in the exact non-dimensional retraction times are observed, compare Figures 4.4(i) and 4.4(k) ($t^*_{retraction} \approx 27.8$) with Figure 4.4(n) ($27.8 < t^*_{retraction} < 30.7$).

Only for the impingement onto deep pools the downward motion of the capillary waves and the subsequent receding and contraction of the cavity takes longer, since for this depth no influence is felt from the bottom of the pool. The capillary waves reach the bottom of the cavity at a time instant at which the cavity is retracting already, Figure 4.4(p). The combination of the downward moving capillary waves and the receding and retracting motion of the cavity leads to the so-called bubble pinch-off, in case the contracting velocity is larger than the retracting velocity, Figure 4.4(t). For each investigated liquid film height a central jet appears after cavity retraction.

In general it can therefore be concluded that the thickness of the liquid film has several influences on the impingement outcome. Since the vertical velocity of the cavity for the initial phase of the impingement process ($t^* \leq 4$) is constant for different film thicknesses, the cavity reaches the bottom of the liquid film sooner for thinner films. This leads to an oblate cavity, having a large cavity diameter, for smaller liquid film thicknesses, whereas for larger film thicknesses the cavity has a more hemispherical shape. Furthermore, the impingement onto thin liquid films results in a higher corona, which can become unstable more easily. However, the time instant at which the cavity retracts is independent of the liquid film thickness and can lead to bubble pinch-off in case of deep pools.

4.1.3 Influence of impinging drop Weber number on cavity shape

Sprays are characterised by many drops having different terminal velocities at impingement. To verify the influence of these terminal drop velocities, the impingement process for three different Weber numbers of the impinging drop are recorded for each liquid film height. The Weber number is changed by changing the value of the terminal velocity of the drop just before impingement. The evolution of the cavity with time is shown in Figure 4.5 for the non-dimensional times inbetween $t^* = -0.7$ and $t^* = 11.9$ and in Figure 4.6 for the times from $t^* = 17.4$ to $t^* = 40.7$. The liquid film height for all three drop Weber numbers shown is kept constant at $h^* = 2$; the liquid for the three cases shown is distilled water.

When comparing the behaviour right after impingement, a few clear differences between the impingement outcomes for the three Weber numbers can be observed. At $t^* = 0.8$ prompt splash is only present at the highest Weber number; for the lower Weber numbers, the kinetic energy of the impinging drops is not high enough to initiate prompt splash. The value of the cavity diameter depends directly on the impinging drop's Weber number, since the more kinetic energy is present at impingement, the easier the surface tension forces, trying to oppose the expansion of the cavity, can be overcome. This means that at the moment of cavity formation, $t^* = 3.1$, the size of the cavity is smaller in diameter for lower Weber numbers. However, the velocity with which the bottom of the cavity penetrates into the liquid film, is independent of the Weber number of the impinging drop. Since the kinetic energy is less for lower Weber numbers, also the corona is seen to reach lower heights and remains stable.

Due to the lower corona, the rim falls back sooner onto the liquid film as a result of gravity, leading to an earlier formation of the capillary waves for lower Weber numbers, compare Figure 4.5(g) for $We = 114$ with Figure 4.5(k) for $We = 225$ and Figure 4.5(n) for $We = 350$. The maximum diameter of the cavity is smaller for lower Weber numbers, since less kinetic energy

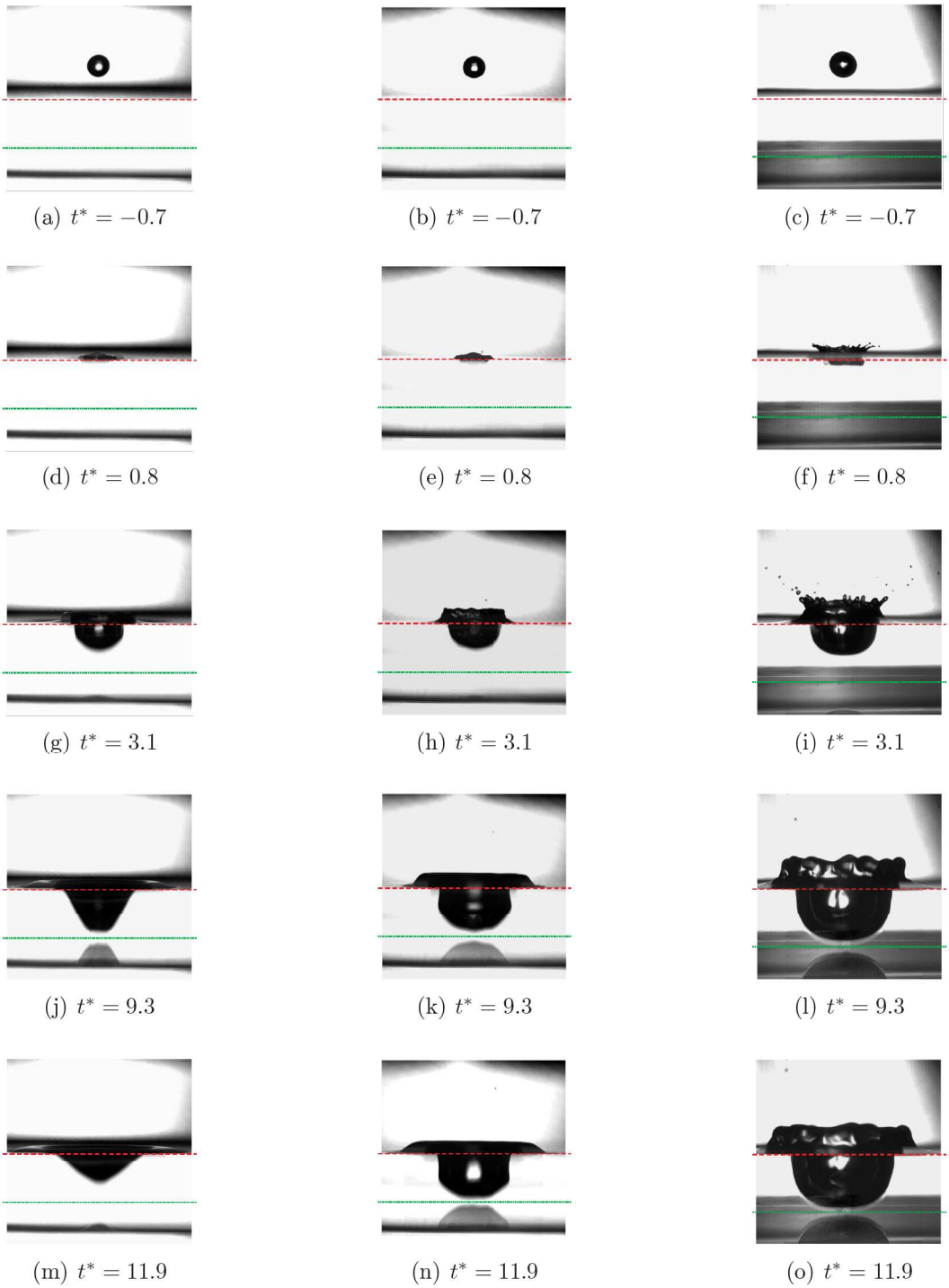

(a) $t^* = -0.7$ (b) $t^* = -0.7$ (c) $t^* = -0.7$

(d) $t^* = 0.8$ (e) $t^* = 0.8$ (f) $t^* = 0.8$

(g) $t^* = 3.1$ (h) $t^* = 3.1$ (i) $t^* = 3.1$

(j) $t^* = 9.3$ (k) $t^* = 9.3$ (l) $t^* = 9.3$

(m) $t^* = 11.9$ (n) $t^* = 11.9$ (o) $t^* = 11.9$

Figure 4.5: Single drop impingement onto a liquid layer of non-dimensional thickness of $h^* = 2$ for different drop impingement Weber numbers. The evolution of the cavity formed by a distilled water drop impingement at non-dimensional time instants between $t^* = -0.7$ and $t^* = 11.9$. The impingement parameters are (left) $D_d = 3.0$ mm and $U_d = 1.7$ m/s ($We = 114$, $Fr = 91$, $Re = 5,061$), (middle) $D_d = 3.0$ mm and $U_d = 2.3$ m/s ($We = 225$, $Fr = 180$, $Re = 7,118$) and (right) $D_d = 3.1$ mm and $U_d = 2.9$ m/s ($We = 350$, $Fr = 273$, $Re = 8,931$)

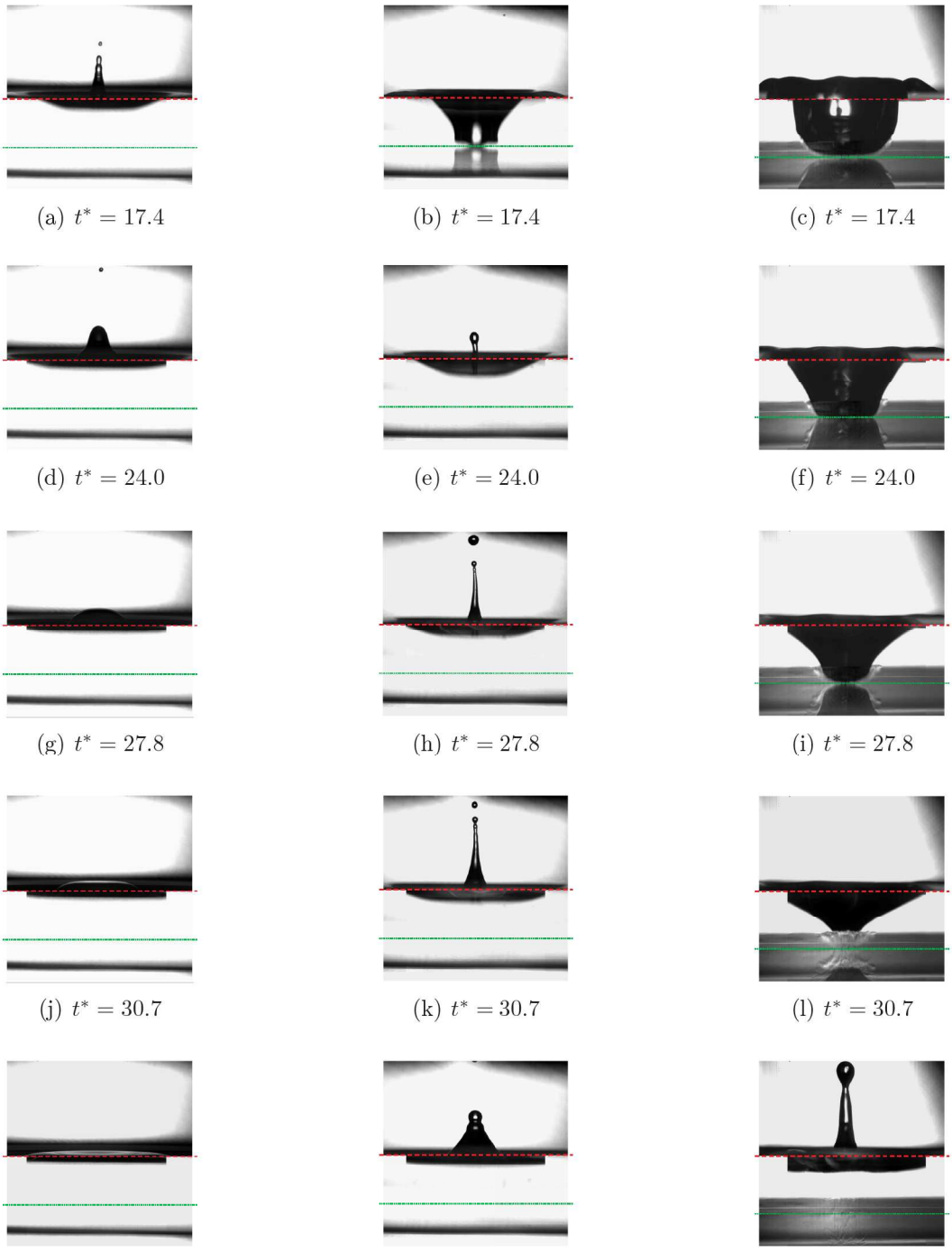

(a) $t^* = 17.4$ (b) $t^* = 17.4$ (c) $t^* = 17.4$

(d) $t^* = 24.0$ (e) $t^* = 24.0$ (f) $t^* = 24.0$

(g) $t^* = 27.8$ (h) $t^* = 27.8$ (i) $t^* = 27.8$

(j) $t^* = 30.7$ (k) $t^* = 30.7$ (l) $t^* = 30.7$

(m) $t^* = 40.7$ (n) $t^* = 40.7$ (o) $t^* = 40.7$

Figure 4.6: Single drop impingement onto a liquid layer of non-dimensional thickness of $h^* = 2$ for different drop impingement Weber numbers. The evolution of the cavity formed by a distilled water drop impingement at non-dimensional time instants between $t^* - 17.4$ and $t^* - 40.7$. The impingement parameters are (left) $D_d = 3.0$ mm and $U_d = 1.7$ m/s ($We = 114$, $Fr = 91$, $Re = 5,061$), (middle) $D_d = 3.0$ mm and $U_d = 2.3$ m/s ($We = 225$, $Fr = 180$, $Re = 7,118$) and (right) $D_d = 3.1$ mm and $U_d = 2.9$ m/s ($We = 350$, $Fr = 273$, $Re = 8,931$)

of the impinging drop can be converted into surface tension energy and dissipated energy after impingement.

The subsequent change of the shape of the cavity from hemispherical to conical, due to the influence of the surface tension forces acting on the cavity, starts earlier for lower Weber numbers, resulting in an earlier receding and retraction of the cavity. At the time instant at which the cavity for the lowest Weber number retracts, $t^* = 11.9$, it is seen that for $We = 225$ the capillary waves are still moving downwards, whereas for the highest Weber number they are just being formed.

The cavity for $We = 225$ retracts around $t^* = 20$ and for $We = 350$ around $t^* = 30$, hence, the differences in retraction times span a range of about $\Delta t = 20$. After cavity retraction a central jet is observed for each of the Weber numbers, but it can be seen clearly that a lower Weber number leads to a thicker central jet with a lower maximum height, compare Figure 4.6(a) with Figure 4.6(k) and Figure 4.6(o). For the lowest Weber number no secondary droplets can be seen to pinch-off the jet, whereas for larger Weber numbers the amount and size of the secondary droplets increase.

Conclusively, a change in Weber number of the impinging drop has a clear influence on the outcome of the impingement process and on the evolution of the cavity shape in time. A higher Weber number leads to a prompt splash, a higher and unstable corona and a cavity with a larger diameter. The velocity with which the cavity penetrates into the liquid layer is independent of the Weber number of the impinging drop, as will be explained in more detail in the next paragraph.

An earlier receding and retraction of the cavity is seen for a lower Weber number, since the kinetic energy of the drop is converted faster into surface tension energy and dissipation energy; hence, the surface tension forces act sooner on the cavity. The central jet that appears after cavity retraction is thicker and reaches a lower maximum height.

4.1.4 Influence of the liquid properties on cavity shape

The last of the parameters changed to investigate the influence on the impingement outcome and the evolution of the shape of the cavity in time, are the liquid properties (surface tension and viscosity). Three different liquid are investigated: distilled water, isopropanol and a mixture of 30 Vol% glycerine and 70 Vol% distilled water. The properties of these liquids are shown in Table 3.1. The evolution of the cavities in time are shown in Figure 4.7 for the non-dimensional times inbetween $t^* = -0.7$ and $t^* = 11.9$ and in Figure 4.8 for the times between $t^* = 17.4$ to $t^* = 40.7$. The liquid film height for all three liquids equals $h^* = 2$; the Weber numbers and Froude numbers of the impinging drops are all in the same range.

When comparing the cavity evolution for the three liquids during the first non-dimensional time instants, not much difference can be seen. At small times after impingement prompt splash and a subsequent unstable corona, leading to finger-like jets and secondary droplets, is only observed for distilled water; for the other liquids the corona is stable and the rim has the shape of a flat torus. Until $t^* = 11.9$ the cavities expand radially with a constant velocity, which is independent of the liquid properties, resulting in the same size of the cavity at different time instants, compare for example Figure 4.7(j) with Figure 4.7(k) and 4.7(l).

Around $t^* = 11.9$ the cavities reach the bottoms of the liquid films. From this moment on, some interesting differences in the cavity behaviour are observed. For distilled water the first capillary waves appear around $t^* = 11.9$, for the glycerine/water mixture around $t^* = 17.4$ and

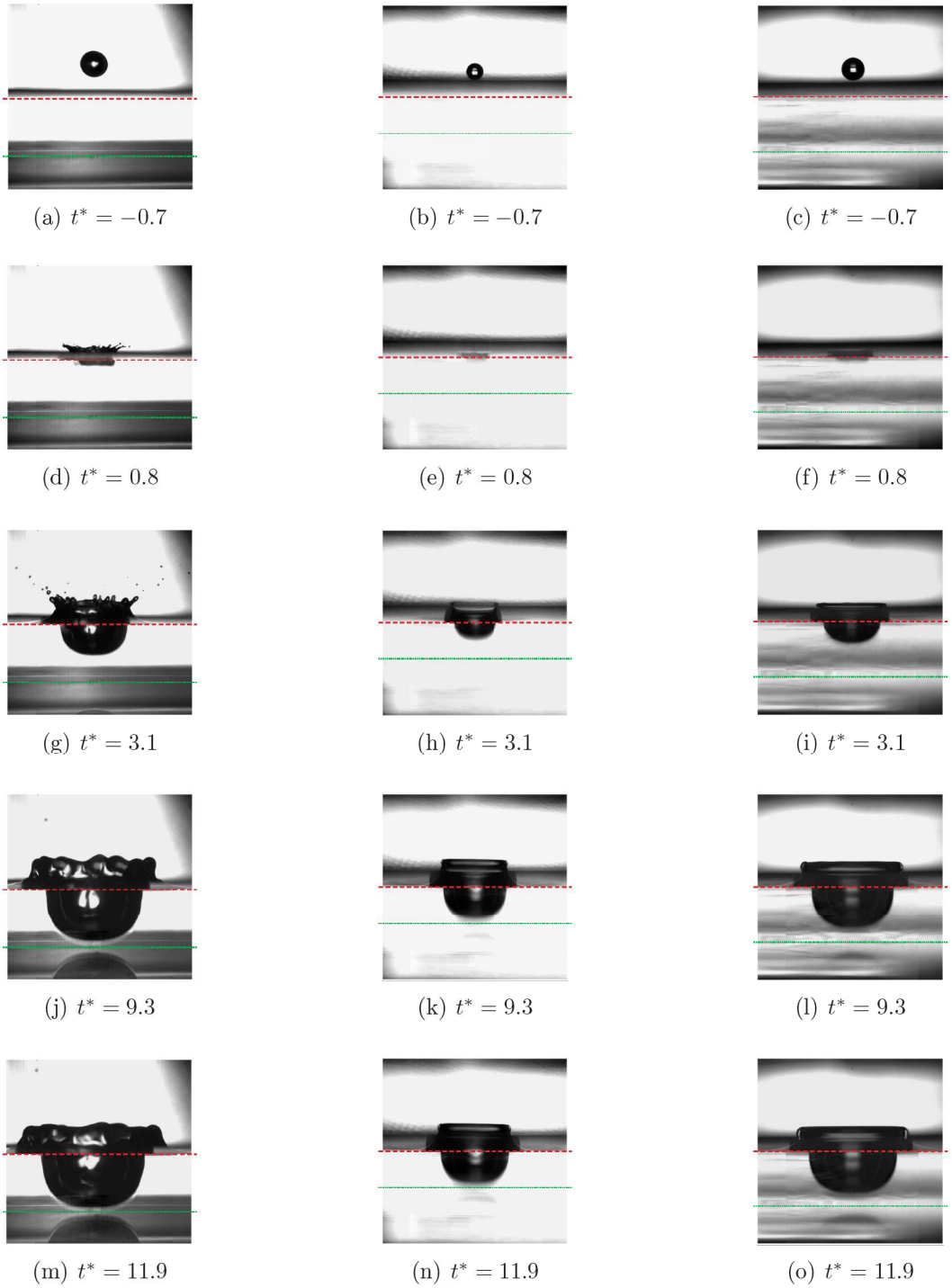

(a) $t^* = -0.7$ (b) $t^* = -0.7$ (c) $t^* = -0.7$

(d) $t^* = 0.8$ (e) $t^* = 0.8$ (f) $t^* = 0.8$

(g) $t^* = 3.1$ (h) $t^* = 3.1$ (i) $t^* = 3.1$

(j) $t^* = 9.3$ (k) $t^* = 9.3$ (l) $t^* = 9.3$

(m) $t^* = 11.9$ (n) $t^* = 11.9$ (o) $t^* = 11.9$

Figure 4.7: Single drop impingement onto a liquid layer of non-dimensional thickness of $h^* = 2$ for different liquids. The evolution of the cavity formed by a drop impingement at non-dimensional time instants between $t^* - -0.7$ and $t^* - 11.9$. The impingement parameters are (left) Distilled water, $D_d = 3.1$ mm and $U_d = 2.9$ m/s ($We = 350$, $Fr = 273$, $Re = 8,931$), (middle) Isopropanol, $D_d = 2.1$ mm and $U_d = 2.7$ m/s ($We = 527$, $Fr = 366$, $Re = 1,982$) and (right) Glycerine/Water, $D_d = 2.7$ mm and $U_d = 3.25$ m/s ($We = 505$, $Fr = 399$, $Re = 561$)

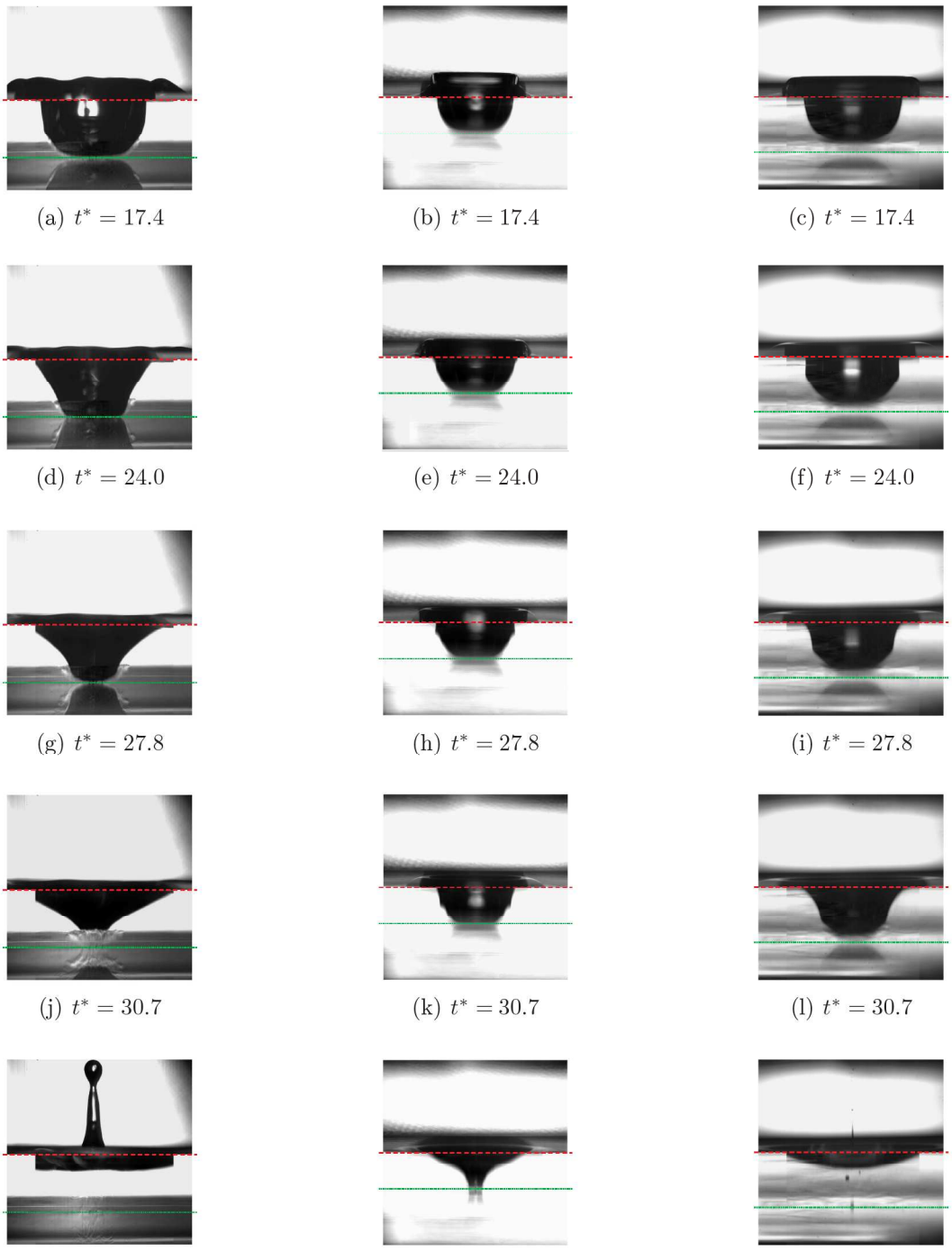

(a) $t^* = 17.4$ (b) $t^* = 17.4$ (c) $t^* = 17.4$

(d) $t^* = 24.0$ (e) $t^* = 24.0$ (f) $t^* = 24.0$

(g) $t^* = 27.8$ (h) $t^* = 27.8$ (i) $t^* = 27.8$

(j) $t^* = 30.7$ (k) $t^* = 30.7$ (l) $t^* = 30.7$

(m) $t^* = 40.7$ (n) $t^* = 40.7$ (o) $t^* = 40.7$

Figure 4.8: Single drop impingement onto a liquid layer of non-dimensional thickness of $h^* = 2$ for different liquids. The evolution of the cavity formed by a drop impingement at non-dimensional time instants between $t^* = 17.4$ and $t^* = 40.7$. The impingement parameters are (left) Distilled water, $D_d = 3.1$ mm and $U_d = 2.9$ m/s ($We = 350$, $Fr = 273$, $Re = 8,931$), (middle) Isopropanol, $D_d = 2.1$ mm and $U_d = 2.7$ m/s ($We = 527$, $Fr = 366$, $Re = 1,982$) and (right) Glycerine/Water, $D_d = 2.7$ mm and $U_d = 3.25$ m/s ($We = 505$, $Fr = 399$, $Re = 561$)

for isopropanol around $t^* = 24.0$. Due to the higher value of the surface tension for distilled water, the rim falls back onto the liquid surface earlier, creating these capillary waves at an earlier time. The size of the capillary waves is directly linked to the surface tension. The lower the surface tension is, the sharper and larger the capillary waves become.

A higher value of the surface tension results in higher forces acting on the surface of the cavity, due to which the cavity recedes and retracts sooner. At the time instant $t^* = 40.7$ the cavity for distilled water has retracted already completely and a central jet has been formed, whereas for the glycerine/water mixture the jet is about to be formed and for isopropanol the cavity is receding and the retracting motion still has to be initiated.

It can be summarised that the influences of the differences in viscosity and surface tension do not become visible until the cavities have reached their maximum diameter and depth. For a lower value of the surface tension, hence a higher Weber number, the capillary waves are more pronounced, the cavity takes longer to recede and its retraction starts at a later time instant.

4.1.5 Comparison with numerics

Figure 4.9 and Figure 4.10 show the evolution of the shape of cavity at different non-dimensional time instants for, respectively, distilled water and isopropanol. The images show a comparison of the shape of the cavity between the experimental recordings (left) and the numerical simulations (right). The impingement parameters are $We = 215$, $Fr = 194$ and $Re = 6,750$ for distilled water and $We = 392$, $Fr = 257$ and $Re = 1,733$ for isopropanol. The numerical simulations presented in both figures are obtained in corporation with Beberovic. The programm *interfoam* is used as flow-solver, which is part of the OpenFOAM packet Version 1.5. The mathematical model is being converted numerically in the framework of a Finite Volume Method (FVM) and has been described in detail by Beberovic *et al.* [10].

The different phases of the mechanism of drop impingement onto a liquid layer of finite thickness have been described in detail in the paragraph above, therefore here only a brief discussion will be given by comparing the experimental data with the numerical simulations. Immediately upon impingement, a circumferential free liquid jet, the so-called corona, is ejected upwards, of which the height, shape and width are a function of the liquid properties, the Weber number and the initial film thickness. It is observed in the numerical simulation that for distilled water the corona is much thicker (Figures 4.9(d) and 4.9(f)) compared to isopropanol (Figures 4.10(d) and 4.10(f)), because of the higher surface tension of distilled water. The cavity penetrates into the liquid film and simultaneously expands in radial direction. The simulations indicate that during the first stages of impingement the cavity has a concave surface, which cannot be observed by the experimental recordings due to the meniscus present at the side walls of the plexiglass container. During the subsequent expansion of the cavity its shape changes to hemispherical. In the penetration phase of the cavity the inertial forces are dominant over the viscous and capillary forces, since the Weber number for both impingements is much higher than unity. It is observed that for both liquids the cavity penetrates into the liquid film with a constant vertical velocity, which equals half of the terminal velocity of the drop just before impingement as will be proven later on in this chapter. In the later discussion of the results for the time evolution of the cavity depth, it will be shown that this penetration velocity is independent of all the investigated drop parameters and film thicknesses.

Due to the capillary forces, acting on the surface of the cavity, the cavity starts its receding motion after having reached the maximum diameter, hereby changing its shape from

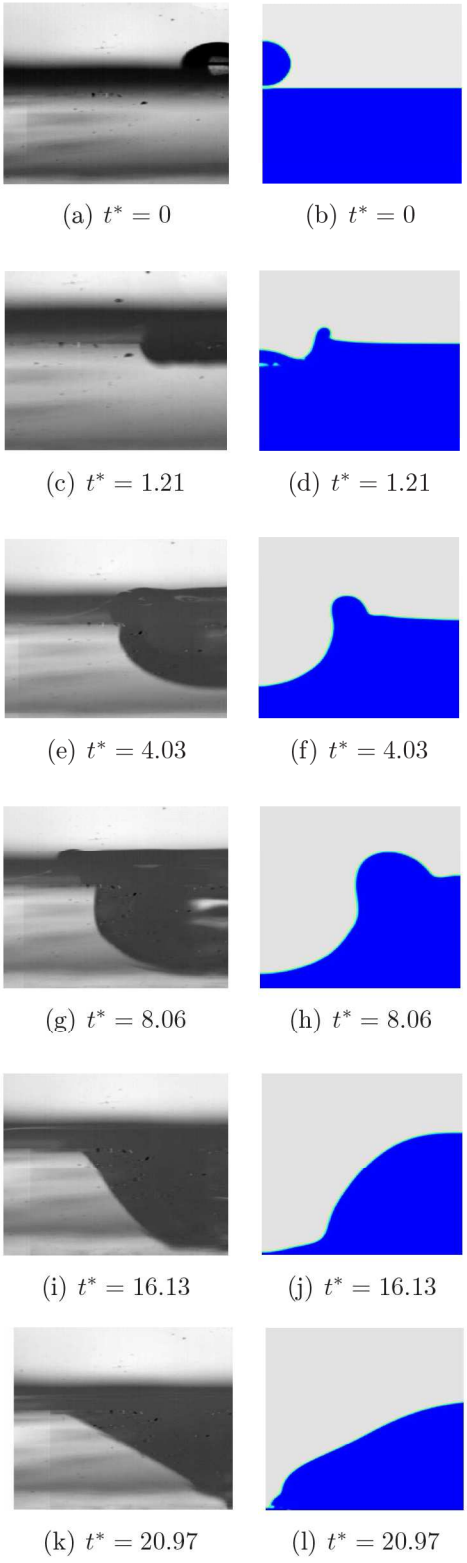

(a) $t^* = 0$ (b) $t^* = 0$

(c) $t^* = 1.21$ (d) $t^* = 1.21$

(e) $t^* = 4.03$ (f) $t^* = 4.03$

(g) $t^* = 8.06$ (h) $t^* = 8.06$

(i) $t^* = 16.13$ (j) $t^* = 16.13$

(k) $t^* = 20.97$ (l) $t^* = 20.97$

Figure 4.9: Single drop impingement onto a liquid layer of non-dimensional thickness $h^* = 2$: (left) experiments and (right) numerical simulations (Beberovic *et. al.* [10]). The evolution of the cavity formed by a distilled water drop ($We = 215$, $Fr = 194$, $Re = 6,750$) impingement at various non-dimensional time instants